

Study on Machinability of Al_2O_3 Ceramic Composite in EDM Using Response Surface Methodology

K. M. Patel¹

Department of Mechanical Engineering,
Institute of Technology,
Nirma University,
Ahmedabad 382 481, India
e-mail: kaushik.patel@nirmauni.ac.in

Pulak M. Pandey

P. Venkateswara Rao

Department of Mechanical Engineering,
Indian Institute of Technology Delhi,
New Delhi 110 016, India

Electric discharge machining (EDM) has been proven as an alternate process for machining complex and intricate shapes from the conductive ceramic composites. Al_2O_3 based electrodischarge machinable Al_2O_3 - SiC_w -TiC ceramic composite is a potential substitute for traditional materials due to their high hardness, excellent chemical, and mechanical stability under a broad range of temperature, and high specific stiffness. The right selection of the machining condition is the most important aspect to take into consideration in the EDM. The present work correlates the inter-relationships of various EDM machining parameters, namely, discharge current, pulse-on time, duty cycle, and gap voltage on the metal removal rate (MRR), electrode wear ratio (EWR), and surface roughness using the response surface methodology (RSM) while EDM of Al_2O_3 - SiC_w -TiC ceramic composite. Analysis of variance is used to study the significance of process variables on MRR, EWR, and surface roughness. The experimental results reveal that discharge current, pulse-on time, and duty cycle significantly affected MRR and EWR, while discharge current and pulse-on time affected the surface roughness. The validation of developed models shows that the MRR EWR and surface roughness of EDM of Al_2O_3 - SiC_w -TiC ceramic can be estimated with reasonable accuracy using the second-order models. Finally, trust-region method for nonlinear minimization is used to find the optimum levels of the parameters. The surface and subsurface damage have also been assessed and characterized using scanning electron microscopy. This study reveals that EDMed material unevenness increases with discharge current and pulse-on time. [DOI: 10.1115/1.4003100]

Keywords: EDM, Al_2O_3 ceramic composite, machinability, RSM, optimization

1 Introduction

Advanced structural ceramics, such as silicon carbide (SiC), silicon nitride (Si_3N_4), alumina (Al_2O_3), and zirconia (ZrO_2), are attractive for many applications due to their very high hardness and strength, wear resistance, resistance to chemical degradation, and low density. Ceramic materials are extensively used in the industrial fields that produce cutting tools, self-lubricating bearings, nozzles, turbine blades, internal combustion engines, heat exchangers, aerospace parts, and as bioceramics. However, they have not achieved their predicted widespread use due to several significant drawbacks, notably their relatively low toughness, the high cost of production, and the difficulty in machining to final tolerances [1]. Conventional sintering and compacting techniques of powder metallurgy, followed by diamond grinding, have been used to machine the ceramic components required in real applications [2]. Ceramic machining can be expensive and difficult when shape is complex and also subjected to generation of surface cracks due their low fracture toughness [3]. EDM is capable of machining complex and intricate shapes regardless of hardness of material, provided that the electrical resistivity is sufficiently low ($<100 \Omega \text{ cm}$) to support sparking. The addition of hard, refractory, and conductive ceramics such as TiN, TiC, TiB_2 , and TiCN

in particulate form to Si_3N_4 , ZrO_2 , and Al_2O_3 has been used as an approach to produce composite with sufficient conductivity for EDM and improved hardness and toughness [4].

Jones et al. [5] used Si_3N_4 based ceramic composite containing TiB_2 for EDM prepared by hot pressing the optimum machining conditions that were identified. The material proved to be excellent for shaping by both die-sinking EDM and wire EDM. Matsuo and Oshima [6] performed wire EDM on conductive zirconia composites containing 23–45 vol % TiC to investigate amount of optimum carbide. Pitman and Huddleston [7] compared the die-sinking EDM characteristics of zirconia based ceramic matrix composite with 30 vol % of titanium nitride under normal sparking and induced arcing conditions and indicated that the major mechanism of material removal was thermal spalling. Nakamura et al. [8] reported surface damage in zirconium diboride (ZrB_2) based composite ceramics induced by EDM. The effects of pulsed current, pulse duration, and duty factor on the strength and the roughness were evaluated.

There have been very few attempts to study EDM of Al_2O_3 based ceramic composites [9–12]. Fu and Li [9] conducted experimental study, in which the pulse current, pulse duration time, and electrical polarity were selected as process parameters that affect surface roughness, MRR, and the variation of fracture strength of Al_2O_3 - Cr_3C_2 composites. They observed that the fracture strength and surface roughness of the composites depend strongly on the pulse current and electrical polarity. The material removal mechanisms of the composites can be categorized as melting at lower pulse current and combined melting and thermal spalling, together with a minor contribution from vaporization, at higher pulse current. Zhang et al. [10] used a hot pressed aluminum

¹Corresponding author.

Contributed by the Materials Division of ASME for publication in the JOURNAL OF ENGINEERING MATERIALS AND TECHNOLOGY. Manuscript received October 13, 2009; final manuscript received August 25, 2010; published online March 3, 2011. Assoc. Editor: Yanyao Jiang.

Table 1 Room temperature mechanical properties of $\text{Al}_2\text{O}_3\text{-SiC}_w\text{-TiC}$ and other bulk ceramics

Ceramic	E (GPa)	H_v (GPa)	K_{IC} ($\text{MPa m}^{0.5}$)
Al_2O_3	356 ± 6	13.3–17.4	3.8
Hot-pressed SiC	430–450	26.9	3–4
TiC	414	35.6	—
$\text{Al}_2\text{O}_3 + 25 \text{ wt } \% \text{ SiC}$	404.1 ± 0.4	21	8.7
AlSiTi	409.6 ± 0.5	19.0–32	9.6 ± 0.6

oxide based ceramics (SG4) for EDM. They demonstrated that the material removal rate, the surface roughness, and the diameter of discharge point increase with increasing pulse-on time and discharge current. They found that longer pulse-on time results into higher surface roughness and generation of thicker resolidified layer with microcracks in the subsurface. In a recent work, Chiang [11] attempted modeling and analysis of the effects of machining parameters on the performance characteristics of EDM process of $\text{Al}_2\text{O}_3\text{-TiC}$ mixed ceramic. Very recently, Chiang and Chang [12] employed gray relational analysis to optimize the multiresponse characteristics of EDM of $\text{Al}_2\text{O}_3\text{-TiC}$ mixed ceramic.

From the literature review presented above, machining of Al_2O_3 based ceramic composites containing conductive compound by spark erosion has been successful but research work has been very limited [9–12] despite the fact that Al_2O_3 ceramic is particularly attractive for engineering applications. The EDM erodable ceramic composites, namely, $\text{Al}_2\text{O}_3\text{-SiC}_w\text{-TiC}$, has been introduced recently, but no EDM machinability study has been reported. The present study is mainly focused on the investigation of EDM machinability of $\text{Al}_2\text{O}_3\text{-SiC}_w\text{-TiC}$ ceramic composite. Therefore, the present work aims to find out the effect of parameters such as discharge current, pulse-on time, duty cycle, and gap voltage on the responses, namely, MRR, EWR, and surface roughness. Experiments have been planned by using central rotatable composite design (CCRD) of experiments. A series of experiments has been performed on die-sinking EDM machine. Analysis of variance (ANOVA) is used to analyze the main effects and to obtain the significant parameters. Three different second-order empirical models have been developed for predicting the MRR, EWR, and surface roughness. The validation of developed models has been carried out and MRR EWR and surface roughness of EDM of $\text{Al}_2\text{O}_3\text{-SiC}_w\text{-TiC}$ ceramic can be estimated with reasonable accuracy using the second-order models. The surface and subsurface damage have also been assessed and characterized using scanning electron microscopy (SEM).

2 Experimental Details

2.1 Composite Fabrication. The alumina based ceramic composite $\text{Al}_2\text{O}_3\text{-SiC}_w\text{-TiC}$, supplied by Industrial Ceramic Technology (Ann Arbor, MI), was fabricated by first mixing and blending of a mixture of 46.1 vol % Al_2O_3 powder, 30.9 vol % SiC whiskers, and 23.0 vol % TiC powder. The SiC whiskers had an initial length of 50 μm and a diameter of $\approx 0.5 \mu\text{m}$. The length decreased by more than a factor of 2 after mixing and blending. The addition of SiC whiskers improves the ability of ceramic composite to resist EDM process induced thermal shocks. Incorporation of TiC powder reduces electrical resistivity ($\rho_{DC} \sim 0.009 \Omega \text{ cm}$ at 20°C) and makes ceramic composite machinable by EDM. It also improves fracture toughness and strength of ceramic composite. The powder mixture was hot pressed in an inert atmosphere at $1700\text{--}1800^\circ\text{C}$. After hot pressing, the density of the composite was 3.915 g/cm^3 , which is $\approx 99\%$ of theoretical density, based on the densities of the constituents [13]. The size of the workpiece is a square of $20 \times 20 \text{ mm}^2$ having a thickness of 5 mm. The mechanical properties of the $\text{Al}_2\text{O}_3\text{-SiC}_w\text{-TiC}$ composite and other bulk ceramics are summarized in Table 1. The mi-

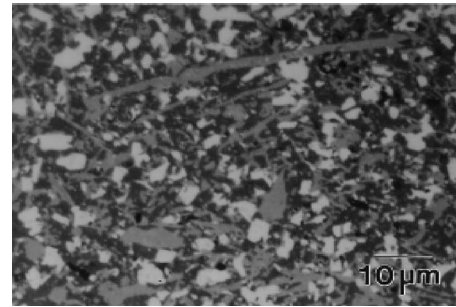


Fig. 1 Microstructure of Al_2O_3 ceramic composite ($\text{Al}_2\text{O}_3\text{-SiC}_w\text{-TiC}$)

crostructure of $\text{Al}_2\text{O}_3\text{-SiC}_w\text{-TiC}$ has been presented in Fig. 1, where the bright grains are TiC particles, the light-gray filaments are the SiC whiskers, and the dark-gray background is the alumina matrix.

2.2 Experimental Design. The design of experiments is a powerful analysis tool for modeling and analyzing the influence of control factors on performance output. The most important stage in the design of experiment lies in the selection of the control factors. It is necessary to choose suitable factors to be varied in the experiment, the ranges over which these factors will be varied, and the specific levels at which runs will be made. EDM is a series of complex physical events with inherent problems and is controlled by a large number of factors. The parameters can be classified as electrical parameters, nonelectrical parameters, electrode based parameters, and workpiece material based parameters. It was necessary to choose a reasonable set of factors to be varied in the experiment. While a smaller set of factors would give a simpler model, a larger number give the model more predictive power. However, the larger number of factors results in more tedious experimentation and analysis. Thus, the selection of factors to some extent should be compromised. Review of literature revealed that among all the factors, discharge parameters such as discharge current, pulse-on time, duty cycle, and gap voltage have most significant influence on the EDM performance. Therefore, it was decided that these four factors be chosen for the present study. It was also found that the volume fraction and size of reinforcements (whiskers and secondary phase) affect the EDM of ceramic composites [5]. Due to nonavailability of $\text{Al}_2\text{O}_3\text{-SiC}_w\text{-TiC}$ ceramic composites with reinforcements in various volume fraction and size, influence of material dependent parameter was not considered in this study.

A series of experiments on EDM of $\text{Al}_2\text{O}_3\text{-SiC}_w\text{-TiC}$ ceramic composite was planned using CCRD. A total of 31 experiments were carried out with independent variables at five different levels. Based on the preliminary experiments conducted by using one variable at a time approach, the range of the discharge current, pulse-on time, duty cycle, and gap voltage were selected as 3–7 A, 10–200 μs , duty cycle 0.24–0.88, and 50–90 V, respectively. When the current was less than 3 A, the observed MRR was insignificant and for the current more than 7 A, $\text{Al}_2\text{O}_3\text{-SiC}_w\text{-TiC}$ ceramic starts disintegrating because of its low fracture toughness resulting in poor surface finish necessitating the selection of the intermediate values as stated above. The range selected for the pulse-on time was commonly used for the EDM of ceramic composites. The levels selected for the duty cycle cover a wide range of duty cycle, whereas the range of gap voltage selected was in accordance to that available on the machine used for the experimentation. Machining time for each workpiece in the experiments has been kept 75 min. The process variables and their levels are summarized in Table 2.

In order to determine the equation of the response surfaces, several experimental designs exist, which approximate the equa-

Table 2 Levels of the independent factors

Factors	Levels				
	-2	-1	0	1	2
Discharge current (A)	3	4	5	6	7
Pulse-on time (μ s)	10	50	100	150	200
Duty cycle	0.24	0.40	0.56	0.72	0.88
Gap voltage (V)	50	60	70	80	90

tion using the smallest number of experiments possible. The most preferred classes of design are the orthogonal first order design and the central composite second-order design. The first order model is acceptable over a narrow range of variables; therefore, the experiments were conducted to obtain second-order model. General second-order surface roughness model in terms of process parameters can be given by [14]

$$\begin{aligned}
 Y = & \beta_0 + \beta_1 X_1 + \beta_2 X_2 + \beta_3 X_3 + \beta_4 X_4 + \beta_{11} X_1^2 + \beta_{22} X_2^2 + \beta_{33} X_3^2 \\
 & + \beta_{44} X_4^2 + \beta_{12} X_1 X_2 + \beta_{13} X_1 X_3 + \beta_{14} X_1 X_4 + \beta_{23} X_2 X_3 \\
 & + \beta_{24} X_2 X_4 + \beta_{34} X_3 X_4
 \end{aligned} \tag{1}$$

where Y is the value of response, namely, MRR, EWR, and surface roughness; $X_1, X_2, X_3,$ and X_4 are the coded values of variables' discharge current, pulse-on time, duty cycle, and gap voltage, respectively. They were obtained using the following transforming equations:

$$X_1 = \frac{I_p - 5}{1} = I_p - 5 \tag{2}$$

$$X_2 = \frac{t_e - 100}{50} \tag{3}$$

$$X_3 = \frac{\eta - 0.56}{0.16} \tag{4}$$

$$X_4 = \frac{U - 70}{10} \tag{5}$$

where, $I_p, t_e, \eta,$ and U are the values of variables' discharge current, pulse-on time, duty cycle, and gap voltage. When the pulse-on time is 10 μ s, it gives a value of a lower level, -1.8 instead of -2. It has been established [14] that small discrepancies in the required factor levels will result in very little difference in the model subsequently developed and the practical interpretation of the results of the experiments would not be seriously affected by the inability of the experimenter to achieve the desired factor levels exactly.

Method of least-squares is used to determine the constant coefficients. Equation (1) represents the response surface; therefore, these designs are also called as response surface designs. In this technique, the main objective is to optimize the response surface that is influenced by various process parameters. Response surface methodology also quantifies the relationship between controllable input parameters and the obtained response surface [14].

2.3 Measurement of MRR, EWR, and Surface Roughness.

Die sinking EDM experiments were carried out on EDM machine (Model PS LEADER ZNC, Electronica, India) using a pulse generator. In all the experiments, kerosene oil was used as dielectric medium. After EDM, $Al_2O_3-SiC_w-TiC$ ceramic composite samples were cleaned with acetone. A high precision electronic weighing balance with least count 10^{-4} g was used to measure the weight loss of EDM specimens and electrodes after each experiment. The surface finish after machining was characterized using profilometer (Talysurf 6, Rank Taylor Hobson, England). A traverse length of 5 mm with a cut-off evaluation length of 0.8

mm was selected. The center line average value of the surface roughness (R_a) is the most widely used surface roughness parameter in industry, which was selected in this study. MRR and EWR are defined as follows:

$$MRR(g/min) = \frac{\text{wear weight of workpiece}}{\text{time of machining}} \tag{6}$$

$$EWR(\%) = \frac{\text{wear weight of electrode}}{\text{wear weight of workpiece}} \times 100 \tag{7}$$

The measured values of MRR, EWR, and surface roughness for each experiment were presented in Table 3.

2.4 Scanning Electron Microscopy. The surfaces of the specimens were examined directly by a SEM EVO 50. The electric discharge machined samples had been mounted on stubs with silver paste before the photomicrographs were taken.

3 Results and Discussions

The work successfully evaluated the feasibility of EDM of newly introduced ceramic composite $Al_2O_3-SiC_w-TiC$. The study reveals that process parameters have strong influence not only on material removal rate but also on electrode wear ratio and surface roughness.

3.1 Material Removal Rate. The main effect plots for MRR are shown in Fig. 2(a). Figure 3 shows the surface plots for MRR prepared with the help of MATLAB software (version 7.0). MRR increases with the increase in discharge current (Fig. 3(a)). This could be due to an increase in both diameter and the depth of the craters, as well as discharge energy at the discharge point, to improve the rate of melting and evaporation. The material removal rate is very less in comparison to that of metals. This is due to very high melting point and low electrical conductivity of $Al_2O_3-SiC_w-TiC$ ceramic composite. Figure 3(a) also shows that MRR decreases with the increase in pulse-on time initially, but after a certain value of pulse-on time, MRR increases. This is due to the fact that, with an increase in pulse-on time, some of the melt resolidify on the workpiece due to lower discharge energy initially, which leads to a decrease in MRR. However, beyond a certain value of pulse-on time, an increase in the discharge energy conducted into the machining gap within a single discharge and causes the MRR to increase [11].

The variation of MRR with duty cycle and discharge current and duty cycle and pulse-on time is shown in Figs. 3(b) and 3(c), respectively. It can be seen that an increase in the duty cycle leads to a slight increase of the MRR. The increase of duty cycle means applying the spark discharge for a longer duration and this causes an increase in MRR.

3.2 Electrode Wear Ratio. Figure 2(b) displays the main effect plots for EWR. Figure 4(a) shows the relationships between the pulse-on time and EWR at various discharge currents. The surface plot reveals that EWR increases with discharge current. The electrical discharge column formed in the machining gap not only removes the unwanted workpiece material but also wears out the electrode. Increase in the discharge current causes more electrical discharge energy to be conducted into the machining gap,

Table 3 Measured responses corresponding to each trial

Exp. No.	Discharge current (X_1) (A)	Pulse-on time (X_2) (μ s)	Duty cycle (X_3)	Gap voltage (X_4) (V)	MRR (mg/min)	EWR (%)	Surface roughness R_a (μ m)
1	1	1	1	-1	4.232	5.04	2.96
2	-1	1	1	1	1.832	4.56	2.66
3	-1	-1	-1	1	0.795	4.39	2.16
4	-1	-1	1	-1	1.640	4.78	2.19
5	0	0	0	0	1.609	5.64	3.15
6	1	-1	1	-1	2.625	5.88	2.35
7	0	0	0	-2	2.072	4.47	2.74
8	1	1	1	1	3.307	5.61	2.96
9	1	-1	1	1	2.333	6.54	2.23
10	0	0	0	0	1.597	5.74	2.84
11	-1	-1	-1	-1	0.772	3.97	2.23
12	0	0	2	0	3.469	6.02	2.31
13	0	0	0	0	1.396	5.62	2.79
14	-1	1	1	-1	2.567	4.23	2.84
15	0	2	0	0	3.087	4.18	3.35
16	-1	1	-1	1	1.460	4.01	2.74
17	1	-1	-1	1	1.225	5.67	2.32
18	-2	0	0	0	0.093	4.28	1.94
19	0	0	0	0	1.604	5.71	2.87
20	0	-2	0	0	1.324	5.56	2.89
21	-1	-1	1	1	1.556	5.09	2.17
22	1	1	-1	1	1.704	5.32	2.84
23	0	0	0	0	1.497	5.46	2.83
24	0	0	0	0	1.444	5.49	2.85
25	1	1	-1	-1	1.672	4.87	3.06
26	1	-1	-1	-1	0.089	5.23	2.34
27	-1	1	-1	-1	1.487	3.56	2.96
28	0	0	0	2	1.195	5.33	2.82
29	0	0	-2	0	1.179	4.09	2.73
30	0	0	0	0	1.341	5.61	2.79
31	2	0	0	0	1.873	6.21	3.03

improving the MRR and increasing the EWR. It is also observed from Fig. 4(a) that an increase in pulse-on time decreases the values of electrode wear ratio. This is due to the fact that the diameter of the discharge column increased with the pulse duration, eventually reducing the energy density of the electrical discharge on the discharge spot [15]. In recent investigations, it has been reported that at longer pulse-on time, the carbon from the decomposition of hydrocarbon-based dielectric liquid deposits on the surface of the tool [16,17]. This deposited layer increases the wear resistance of the tool and reduces EWR. The effects of duty cycle, discharge current, duty cycle, and pulse-on time on the value of EWR are presented in Figs. 4(b) and 4(c). It shows that the value of EWR increases with an increase of the duty cycle. An increase in duty cycle lead to generation of higher spark energy, which causes an increase of electrode wear, which eventually resulted into higher EWR. It can be seen from the main effects plot (Fig. 2(b)) that the gap voltage does not influence the EWR to a great extent.

3.3 Surface Roughness. Figure 2(c) displays the main effect plots for surface roughness. It can be seen that the discharge current and pulse-on time are significant parameters affecting surface roughness. The surface plot presented in Fig. 5 shows the relationships between discharge current and surface roughness at various pulse-on time. An increase in discharge current increases the surface roughness, while EDM of $Al_2O_3-SiC_w-TiC$ composite. The discharge energy density and the impulsive force increase with the discharge current and result in the formation of deeper and larger discharge craters. It increases both MRR and surface roughness. Moreover, at higher discharge current, EDM of $Al_2O_3-SiC_w-TiC$ composite is subjected to generation of micropores due its low fracture toughness and low thermal shock resistance, which causes the surface finish to deteriorate. Thus, the quality of the machined surface gradually declines and the surface roughness increases as

the discharge current increases. The small improvement in surface finish has been observed beyond a discharge current of 6 A. This may be due to the presence of a sufficient amount of aluminum and silicon particle machining debris in the dielectric fluid, which modifies the plasma channel. The plasma channel becomes enlarged and widened [18]. The electric density decreases; hence, sparking is uniformly distributed among the powder particles. As a result, an even more uniform distribution of the discharge takes place, which causes uniform erosion (shallow craters) on the workpiece. This results in improved surface finish. An increase in pulse-on time increases the surface roughness. This is due to the expansion of plasma channel, which results into a wider contact zone of discharging. This reduces both energy density and the impulsive force. The melted debris cannot be removed completely due to reduction in impulsive force and forms an apparent globulelike recast layer, which ultimately results in degradation of the surface roughness. In the case of EDM of $Al_2O_3-SiC_w-TiC$, the micropores and fine pock mark formation are also observed with prolonged pulse-on time. Besides, reduction in the removal of debris and the carbon accumulation on machined surface, micropores, and fine pock mark formation also attribute to further increase in surface roughness with an increase in pulse-on duration. It is observed that discharge current, pulse-on time, and duty cycle significantly influenced the MRR and EWR, while discharge current and pulse-on time influenced the surface roughness.

3.4 Surface Morphology. During the EDM process, results in bombardment of high energetic (kinetic) electrons on the electrode surface, the spot attains high temperature (about 10,000°C) especially with materials of low thermal conductivity. At this high temperature, material at that spot melts and vaporizes leaving a crater on the surface. However, small amount of the molten material cools rapidly under the effects of the dielectric fluid. The rapid heating and cooling effect generates a highly distinctive sur-

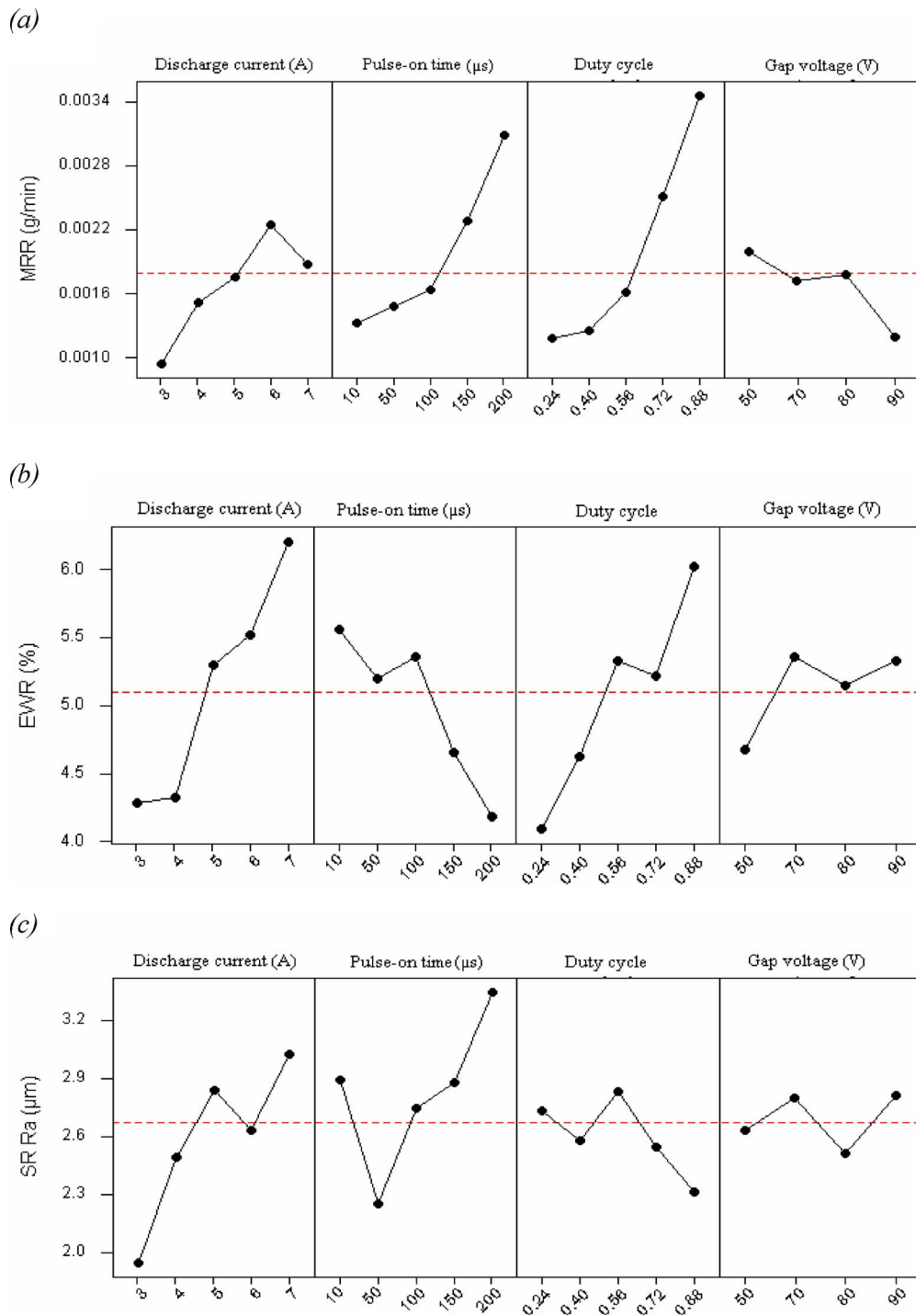


Fig. 2 Main effects plots: (a) main effects for MRR, (b) main effects for EWR, and (c) main effects for surface roughness

face morphology on electrical discharge machined surfaces.

The SEM micrographs of the EDM machined surfaces at a pulse-on time of 50 μ s for various currents are given in Fig. 6. The EDM surface is characterized by an uneven fused structure, globules of debris, shallow craters, and micropores. Micrographs also show the formation of bright TiC layer on the machined surface. SEM examination of the EDM machined surface shows no surface cracks. It can be seen from surface micrographs shown in Figs. 6(a) and 6(b) that the surface roughness increases with an increase in discharge current. This increase could be due to the increase in deeper and larger discharge craters with other irregu-

larities as the pulse current increases. An increase in discharge current forms micropores due to low fracture toughness and thermal shock resistance of $\text{Al}_2\text{O}_3\text{-SiC}_w\text{-TiC}$ ceramic composite. Improvement in surface roughness was observed at discharge current of 7 A for a 50 μ m pulse-on time (micrograph of Fig. 6(c)). The decrease in surface roughness may be due to the enhanced TiC deposition and could also due to the uniform sparking resulting from the presence of Al and Si particles (machining debris) in the kerf.

The SEM micrographs of the EDM machined surfaces at a

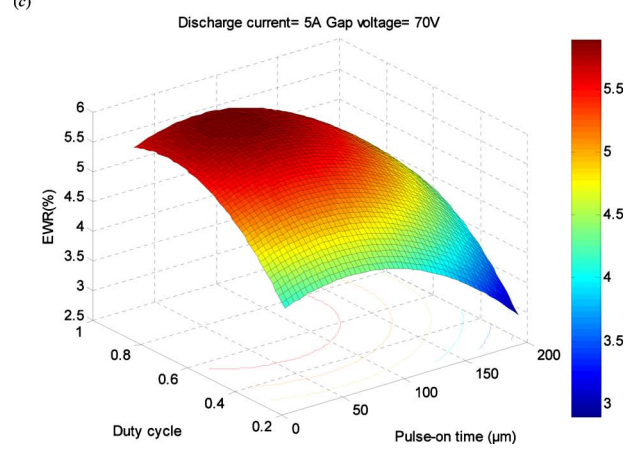
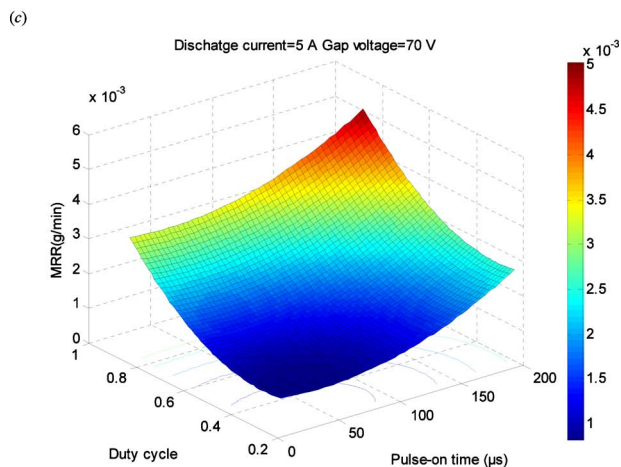
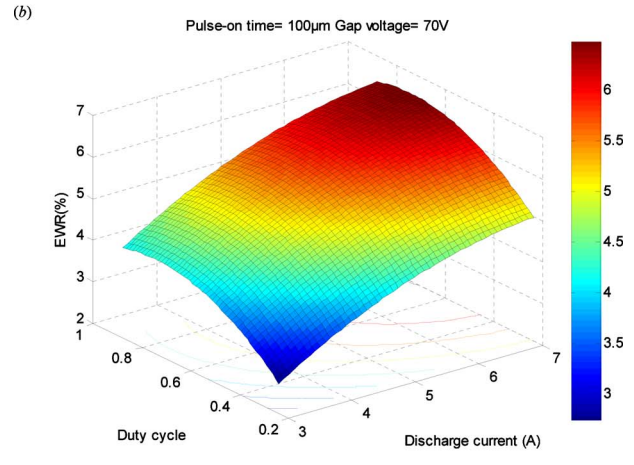
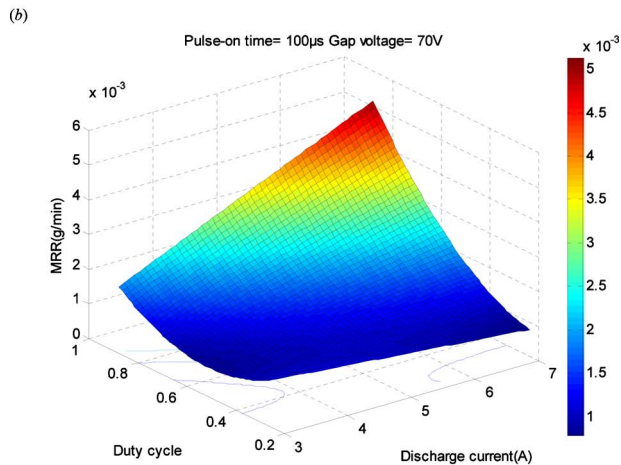
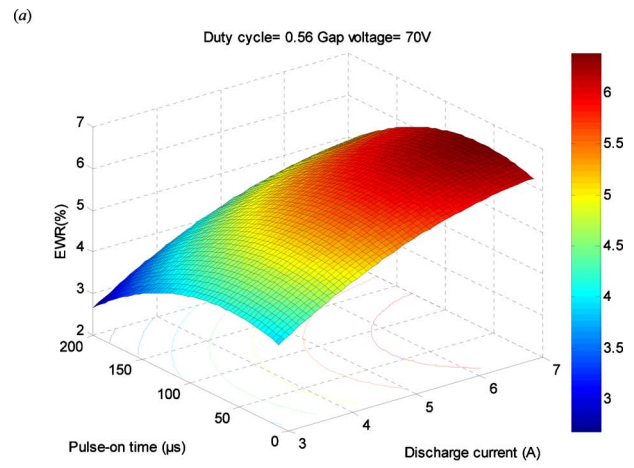
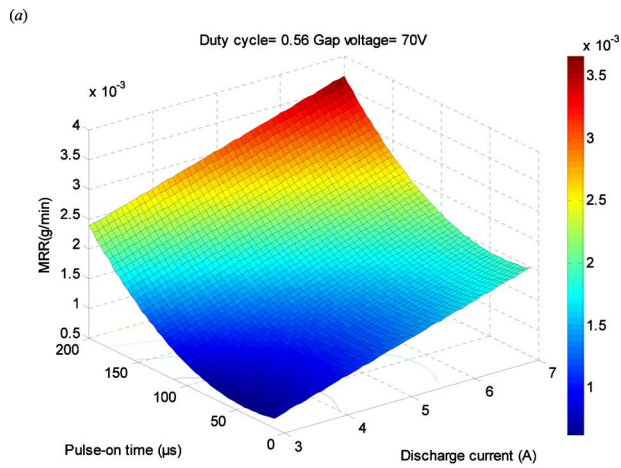


Fig. 3 Response surfaces for MRR

Fig. 4 Response surfaces for EWR

pulse-on time of 200 μs for various currents of normal cutting mode are shown in Fig. 7. On comparison of the micrographs shown in Figs. 6 and 7, it can be seen that the surface irregularities increase with an increase in pulse-on time. The increase in surface unevenness is more predominant with an increase in pulse-on time in comparison to an increase in discharge current. This may be due to the plasma channel expansion with the increase in pulse-on time. It widens the contact zone of discharge and subsequently reduces both energy density and the impulsive force. The melted debris might not be removed completely due to reduction in impulsive force and forms an apparent globulelike recast layer to degrade the surface roughness. These effects be-

come more pronounced as the pulse-on time increases. Besides, a reduction in the removal of debris and carbon accumulation on machined surface [18], micropores, and fine pock mark formation also attribute to further increase in surface roughness with an increase in pulse-on time.

Subsurface damage and recast layer of the EDMed specimens were also investigated and is presented in Fig. 8. When the spark eroded area was observed for subsurface damage, melt flow of the recast layer was observed. The extremely fine cracks were filled by the recast layer. It can be seen from the micrographs that the thickness of the recast layer varies for different values of pulse-on time (Figs. 8(a) and 8(b)). The recast layer thickness is influenced by the pulse-on time and increases as the pulse-on time increases.

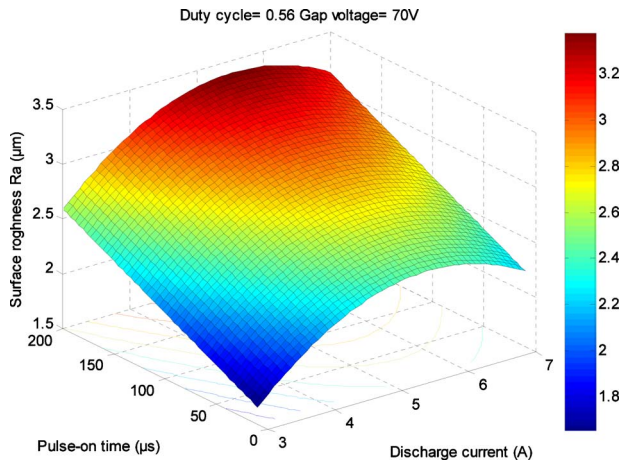


Fig. 5 Response surface for surface roughness

This can be explained by the fact that the amount of material that can be flushed away by the dielectric is constant while EDM occurs. Therefore, as more heat is transferred into the sample as the pulse-on time increases, the dielectric is increasingly unable to clear away the material debris, and so it builds up on the surface

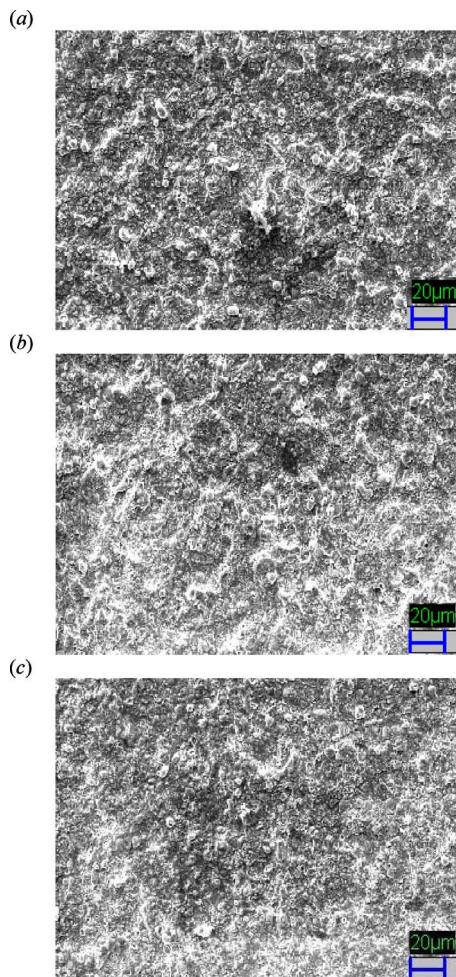


Fig. 6 EDMed surface characteristics of $\text{Al}_2\text{O}_3\text{-SiC}_w\text{-TiC}$ ceramic composite under a duty cycle of 0.72, a gap voltage of 70 V, and a pulse-on time of 50 μs : (a) discharge current of 3 A, (b) discharge current of 5 A, and (c) discharge current of 7 A

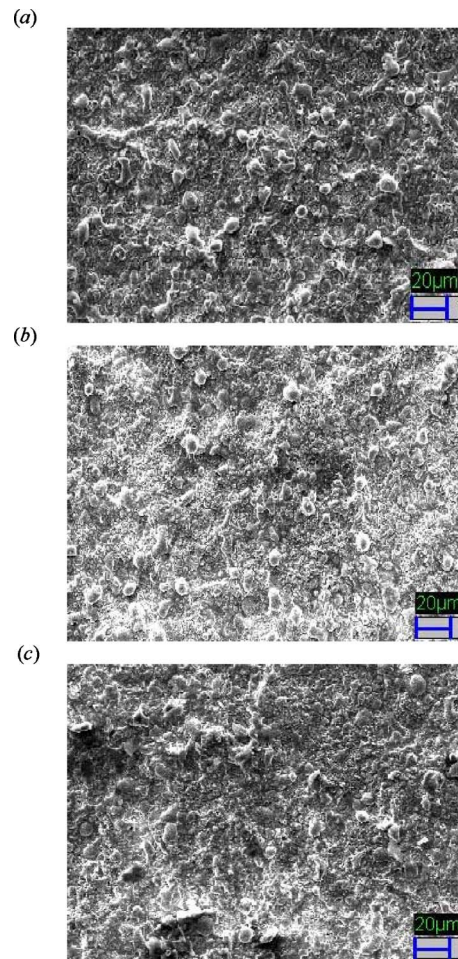


Fig. 7 EDMed surface characteristics of $\text{Al}_2\text{O}_3\text{-SiC}_w\text{-TiC}$ ceramic composite under a duty cycle of 0.72, a gap voltage of 70 V, and a pulse-on time of 200 μs : (a) discharge current of 3 A, (b) discharge current of 5 A, and (c) discharge current of 7 A

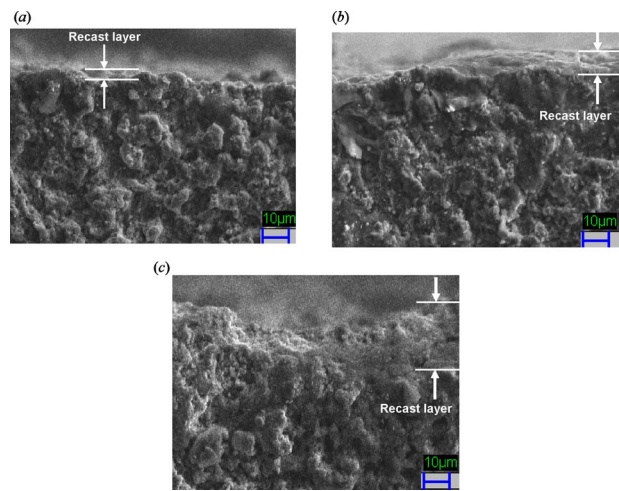


Fig. 8 SEM. Micrographs at a duty cycle of 0.72 and a gap voltage of 70 V: (a) 3 A/50 μs , (b) 7 A/50 μs , (c) 7 A/200 μs , where the micrographs (b) and (c) qualitatively show variation in the thickness of the recast layer for different values of pulse-on time

Table 4 ANOVA table for MRR (after elimination)

Source	SS	DF	MS	F value	P value	R ²	Remark
Regression	1.97 × 10 ⁻⁰⁵	9	2.19 × 10 ⁻⁰⁶	62.3931	<0.0001	0.9636	F _{0.01,9,21} =3.40, F > F _{0.01,9,21}
Linear	1.61 × 10 ⁻⁰⁵	4	4.02 × 10 ⁻⁰⁶				Model is adequate and lack of fit is insignificant
Square	2.10 × 10 ⁻⁰⁶	2	1.05 × 10 ⁻⁰⁶				
Interactions	1.49 × 10 ⁻⁰⁶	3	4.96 × 10 ⁻⁰⁷	3.73	0.057		
Residual error	7.36 × 10 ⁻⁰⁷	21	3.51 × 10 ⁻⁰⁸				
Lack-of-fit	6.65 × 10 ⁻⁰⁷	15	4.43 × 10 ⁻⁰⁸				
Pure error	7.14 × 10 ⁻⁰⁸	6	1.19 × 10 ⁻⁰⁸				
Total	2.04 × 10 ⁻⁰⁵						

of the sample. During the subsequent cooling, this material resolidifies to form the recast layer, the depth of which depends on the volume of debris, which is left on the sample surface during machining.

4 ANOVA and Effects of the Factors

In order to find out the statistical significance of various factors such as discharge current, pulse-on time, duty cycle, and gap voltage impact velocity on MRR, EWR, and surface roughness, ANOVA is performed on experimental data. Tables 4–6 show the results of the ANOVA for MRR, EWR, and surface roughness.

4.1 Modeling of MRR. MRR model has been obtained by analyzing the data presented in Table 3 and is given below as Eq. (8),

$$\begin{aligned} \text{MRR} = & 0.001505 + 0.000323X_1 + 0.000414X_2 + 0.000611X_3 \\ & - 0.00014X_4 + 0.000174X_2^2 + 0.000204X_3^2 + 0.000245X_1X_3 \\ & - 0.0001X_2X_4 - 0.00015X_3X_4 \end{aligned} \quad (8)$$

ANOVA is used to check the adequacy of developed model. ANOVA of this response surface is presented in Table 4. *F*-ratio of the predictive model is calculated and compared with the standard tabulated value of *F*-ratio for a specific confidence interval. The *F*-value of the model shows that the model is adequate at 99% confidence level. The duty cycle is found to be the most significant factor influencing the MRR with contribution of 43.92%, which is followed by pulse-on time and discharge current with contributions of 20.20% and 12.30%, respectively.

4.2 Modeling of EWR. The ANOVA table for the reduced quadratic model for EWR is shown in Table 5. It can be seen from Table 5 that this model is adequate at 99% confidence level. The ANOVA of experimental data shows that the relative contributions of discharge current, pulse-on time, and duty cycle on EWR are 42.29%, 11.85%, and 17.22%, respectively. The modified EWR model is therefore given as follows:

$$\begin{aligned} \text{EWR} = & 5.61 + 0.559583X_1 - 0.29625X_2 + 0.357083X_3 \\ & + 0.222917X_4 - 0.10719X_1^2 - 0.20094X_2^2 - 0.15469X_3^2 \\ & - 0.19344X_4^2 \end{aligned} \quad (9)$$

4.3 Modeling of Surface Roughness. Second-order model was obtained for surface roughness data presented in Table 6. The improved model after neglecting the terms, which have insignificant effect on the surfaces roughness, is obtained as

$$\begin{aligned} R_a = & 2.85756 + 0.136871X_1 + 0.248329X_2 - 0.0469X_3 \\ & - 0.12249X_1^2 - 0.11378X_3^2 \end{aligned} \quad (10)$$

ANOVA for the response surface given by Eq. (10) is presented in Table 6. It is clear from the *F*-test that the model is adequate at 99% confidence level as the *F*-value of model is higher than the tabulated *F*-value and lack of fit is insignificant. The two significant main effects of factors affecting the surface roughness are discharge current and pulse-on time with the contributions of 11.91% and 39.19% respectively, whereas the second-order effects of both the discharge current and duty cycle also contribute significantly by 12.49% and 10.85% respectively.

Table 5 ANOVA table for EWR (after elimination)

Source	SS	DF	MS	F value	P value	R ²	Remark
Regression	17.11171	8	2.138963	71.41066	<0.0001	0.9613	F _{0.01,8,22} =3.45, F > F _{0.01,8,22}
Linear	13.87435	4	3.468588				Model is adequate and lack of fit is insignificant
Square	3.237361	4	0.80934	3.44	0.0674		
Residual error	0.658963	22	0.029953				
Lack-of-fit	0.594163	16	0.037135				
Pure error	0.0648	6	0.0108				
Total	17.77067						

Table 6 ANOVA table for surface roughness (after elimination)

Source	SS	DF	MS	F value	P value	R ²	Remark
Regression	3.152882	5	0.630576	28.24	<0.0001	0.8496	F _{0.01,5,25} =3.86, F > F _{0.01,5,25}
Linear	2.233552	3	0.744554				Model is adequate and lack of fit is insignificant
Square	0.919326	2	0.459663	2.71	0.1103		
Residual error	0.558137	25	0.022325				
Lack-of-fit	0.499924	19	0.026311				
Pure error	0.058212	6	0.009702				
Total	3.711020						

Table 7 Confirmation Experiments

Exp. No.	Machining conditions				MRR (g/min)		EWR (%)		Surface roughness R_a (μm)	
	Discharge current (A)	Pulse-on time (μs)	Duty cycle	Gap voltage (V)	Expt.	Predicted	Expt.	Predicted	Expt.	Predicted
1	5	200	0.56	70	0.003087	0.003031 ± 0.000587	4.18	4.2137 ± 0.54	3.35	3.3542 ± 0.460
2	5	100	0.88	70	0.003469	0.003543 ± 0.000587	6.02	5.705 ± 0.54	2.31	2.3086 ± 0.460
3	3	150	0.56	80	0.001445	0.001202 ± 0.000587	3.78	3.594 ± 0.54	2.77	2.3422 ± 0.460
4	6	10	0.40	70	0.001198	0.001044 ± 0.000587	5.56	5.339 ± 0.54	2.59	2.3084 ± 0.460

4.4 Validation of Developed Models. The second-order models for different responses, namely, MRR, EWR, and surface roughness, were validated using the chi square test. The calculated chi square values of the models for the MRR, EWR, and surface roughness are 3.90×10^{-04} , 0.1296, and 0.3595, respectively. The tabulated value at χ^2 0.005 is 14.458, which indicates that 99.5% of the variability in MRR, EWR, and surface roughness is explained by these models. Therefore, the MRR, EWR, and surface roughness of EDM of $\text{Al}_2\text{O}_3\text{-SiC}_w\text{-TiC}$ ceramic can be estimated with reasonable accuracy using the second-order models.

5 Confirmation Experiments

Due to the experimental error, the estimated parameters and hence the estimated MRR, EWR, and surface roughness are subjected to uncertainty. The precision of responses were estimated by calculating confidence interval. The confidence interval for the predicted response is $Y \pm \Delta Y$, where ΔY is given by

$$\Delta Y = t_{\alpha/2, DF} \sqrt{V_e} \tag{11}$$

Here Y is denoted for the responses, namely, MRR, EWR, and surface roughness, t is the value of horizontal coordinate on t -distribution corresponding to the specified degree of freedom (DF), α is the level of confidence interval, and V_e is the variance of error of the predicted response. The value of α is taken as 0.005. The values of ΔMRR , ΔEWR , and ΔR_a for MRR, EWR, and surface roughness models are calculated as 5.873×10^{-04} g/min, 0.54%, and 0.460 μm , respectively.

In order to verify the adequacy of the model developed, four confirmation experiments were performed, as shown in Table 7. The test conditions for first two confirmation experiments are among the cutting conditions that were part of the original CCRD designed experiment. The remaining two confirmation experiments are within the range of the levels defined for the various parameters. The predicted values and the associated confidence interval are based on the developed models. The predicted values and the actual experimental values are presented and compared in Table 7. It can be seen that developed models can predict the MRR, EWR, and surface roughness accurately within 99.5% confidence interval.

6 Factor Settings for Minimum Surface Roughness

In this study, an attempt was made to derive optimal control settings factors for minimization of surface roughness. The single objective optimization requires quantitative determination of the relationship between surface roughness with combination of control factors. The second-order surface roughness model obtained is given as

$$R_a = -2.61128 + 1.36177I_p + 0.00496t_e + 4.67968\eta - 0.12249I_p^2 - 4.44\eta^2 \tag{12}$$

(in actual factors).

The problem of constrained optimization using a developed surface roughness model for EDM of $\text{Al}_2\text{O}_3\text{-SiC}_w\text{-TiC}$ ceramic composite was formulated and is given by

$$\text{minimize}(R_a)$$

subjected to

$$3(A) \leq I_p \leq 7(A)$$

$$10(\mu\text{s}) \leq t_e \leq 200(\mu\text{s})$$

$$0.24 \leq \eta \leq 0.88$$

Trust-region method for nonlinear minimization was used to find the optimum levels of the parameters. Optimization tool box of MATLAB 7.0 was used for carrying out the optimization.

A standard function of MATLAB 7.0, namely, *fmincon*, that can handle a large-scale optimization problem with nonlinear equality, as well as inequality constraint, is used for the purpose. The obtained process parameters, which give minimum surface roughness, are presented in Table 8. This optimization methodology can be used to determine minimum surface roughness with given constraints and also identifies the conditions at which the EDM operation must be carried out in order to get the better surface finish. The application of a trust region method to obtain optimal machining conditions for EDM of ceramic composite will be quite useful at the computer-aided process planning (CAPP) stage in the production of electric discharge machined parts. These data are currently not available for EDM of ceramic composites.

7 Conclusions

In the present study, the influence of machining parameters on MRR, EWR, and surface roughness during EDM of $\text{Al}_2\text{O}_3\text{-SiC}_w\text{-TiC}$ ceramic composite using copper electrode was investigated. Mathematical models were developed to predict MRR, EWR, and surface roughness by correlating the input parameters, namely, discharge current, pulse-on time, duty cycle, and gap voltage. Significant parameters were identified for each response. ANOVA was used to establish adequacy of the developed models. The developed models have also been validated using chi square test. The results show that second-order models developed for MRR and EWR are statistically significant.

The individual influences of all process parameters on the MRR, EWR, and surface roughness were analyzed based on the

Table 8 Optimum process parameters for minimizing surface roughness

Discharge current (A)	Pulse-on time (μs)	Duty cycle	Gap voltage (V)	Calculated SR, R_a at optimum parameters (μm)	Experimental SR, R_a at optimum parameters (μm)
3	10	0.88	Insignificant	1.0483	1.33

developed mathematical models. The experimental results reveal that discharge current, pulse-on time, and duty cycle significantly affect the MRR and EWR, while discharge current and pulse-on time affect the surface roughness. Confirmation experiments were conducted at various test conditions to show that the developed models can predict MRR, EWR, and surface roughness values accurately.

It is concluded from the surface morphology of EDMed material unevenness increases with discharge current and pulse-on time. The thickness of the recast layer increases with the pulse-on time. This study showed that $\text{Al}_2\text{O}_3\text{-SiC}_w\text{-TiC}$ could be efficiently machined without causing a significant loss to the surface integrity.

The two-stage effort of obtaining a surface roughness model by response surface methodology and optimization of this model by a trust region method resulted in a useful method of obtaining process parameters in order to attain the improved surface quality. Minimum surface roughness was determined with given constraints. The cutting conditions identified for minimum surface roughness were discharge current, pulse-on time, duty cycle, and gap voltage of 7 A, 50 μs , 0.80, and 50 V respectively.

Acknowledgment

The authors would like to express their sincere thanks to Mr. John J. Schuldies, President, Industrial Ceramic Technology Inc., Ann Arbor, MI, for supplying the work material.

Nomenclature

F	= Fischer value
I_p	= discharge current (A)
R_a	= actual surface roughness (μm)
t_e	= pulse-on time (μs)
U	= gap voltage (V)
X_1	= coded value of discharge current
X_2	= coded value of pulse-on time
X_3	= coded value of duty cycle
X_4	= coded value of gap voltage
Y	= process yield
$\beta_i, \beta_{ii}, \beta_{ij}$	= constant coefficients
ε	= random error
η	= duty cycle
χ^2	= chi square

References

- [1] Xu, H. H. K., Jahanmir, S., and Ives, L. K., 1996, "Material Removal and Damage Formation Mechanisms in Grinding Silicon Nitride," *J. Mater. Res.*, **11**(7), pp. 1717–1724.
- [2] Sarkar, B. R., Doloi, B., and Bhattacharyya, B., 2006, "Parametric Analysis on Electro Chemical Discharge Machining of Silicon Nitride Ceramics," *Int. J. Adv. Manuf. Technol.*, **28**, pp. 873–881.
- [3] Tuersley, I. P., Jawaid, A., and Pashby, I. R., 1994, "Review: Various Methods of Machining Advanced Ceramic Materials," *J. Mater. Process. Technol.*, **42**, pp. 377–390.
- [4] Put, S., Vleugels, J., Biest, O. V., Trueman, C., and Huddleston, J., 2001, "Die Sink Electro Discharge Machining of Zirconia Based Composites," *Br. Ceram. Trans.*, **100**(5), pp. 207–213.
- [5] Jones, A. H., Trueman, C., Dobedoe, R. S., Huddleston, J., and Lewis, M. H., 2001, "Production and EDM of $\text{Si}_3\text{N}_4\text{-TiB}_2$ Ceramics Composites," *Br. Ceram. Trans.*, **100**(2), pp. 49–54.
- [6] Matsuo, T., and Oshima, E., 1992, "Investigation on the Optimum Carbide Content and Machining Condition for Wire EDM of Zirconia Ceramics," *CIRP Ann.*, **41**(1), pp. 231–234.
- [7] Pitman, A., and Huddleston, J., 2000, "Electrical Discharge Machining of ZrO_2/TiN Particulate Composite," *Br. Ceram. Trans.*, **99**(2), pp. 77–84.
- [8] Nakamura, M., Shigematsu, I., Kanayama, K., and Hirai, Y., 1991, "Surface Damage in ZrB_2 Based Composite Ceramics Induced by Electro Discharge Machining," *J. Mater. Sci.*, **26**, pp. 6078–6082.
- [9] Fu, C.-T., and Li, A., 1994, "The Dependence of Surface Damage Induced by Electrical Discharge Machining on the Fracture Strength of $\text{Al}_2\text{O}_3\text{-Cr}_3\text{C}_2$ Composites," *Mater. Chem. Phys.*, **39**, pp. 129–135.
- [10] Zhang, J. H., Lee, T. C., and Lau, W. S., 1997, "Study on the Electro Discharge Machining of Hot Pressed Aluminium Oxide Based Ceramics," *J. Mater. Process. Technol.*, **63**, pp. 908–912.
- [11] Chiang, K., 2008, "Modeling and Analysis of the Effects of Machining Parameters on the Performance Characteristics in the EDM Process of $\text{Al}_2\text{O}_3\text{+TiC}$ Mixed Ceramic," *Int. J. Adv. Manuf. Technol.*, **37**, pp. 523–533.
- [12] Chiang, K., and Chang, F., 2007, "Applying Grey Forecasting Method for Fitting and Predicting the Performance Characteristics of an Electroconductive Ceramic ($\text{Al}_2\text{O}_3\text{+30%TiC}$) During Electrical Discharge Machining," *Int. J. Adv. Manuf. Technol.*, **33**, pp. 480–488.
- [13] Smirnov, B. I., Nikolaev, V. I., Orlova, T. S., Shpeizman, V. V., Arellano-Lopez, A. R. D., Goretta, K. C., Singh, D., and Routbort, J. L., 1998, "Mechanical Properties and Microstructure of an $\text{Al}_2\text{O}_3\text{-SiC-TiC}$ Composite," *Mater. Sci. Eng., A*, **242**, pp. 292–295.
- [14] Montgomery, D. C., 1991, *Design and Analysis of Experiments*, Wiley, Singapore.
- [15] Lin, Y. C., Cheng, C. H., Su, B. L., and Hwang, L. R., 2006, "Machining Characteristics and Optimization of Machining Parameters of SKH 57 High Speed Steel Using Electrical Discharge Machining Based on Taguchi Method," *Mater. Manuf. Processes*, **21**, pp. 922–929.
- [16] Chen, Y., and Mahdavian, S. M., 1999, "Parametric Study into Erosion Wear in a Computer Numerical Controlled Electro Discharge Machining Process," *Wear*, **236**, pp. 350–354.
- [17] Ozgedik, A., and Cogun, C., 2006, "An Experimental Investigation of Tool Wear in Electric Discharge Machining," *Int. J. Adv. Manuf. Technol.*, **27**, pp. 488–500.
- [18] Wu, K. L., Yan, B. H., Huang, F. Y., and Chen, S. C., 2005, "Improvement of Surface Finish on SKD Steel Using Electro Discharge Machining With Aluminum and Surfactant Added Dielectric," *Int. J. Mach. Tools Manuf.*, **45**, pp. 1195–1201.